International Journal of Fracture **79:** 65–83, 1996.

Two-parameter characterization of the near-tip stress fields for a bi-material elastic–plastic interface crack

Z.L. ZHANG[1], M. HAUGE[1] and C. THAULOW[2]
[1] *SINTEF Materials Technology, N-7034 Trondheim, Norway*
[2] *NTNU, Department of Machine Design and Materials Technology, N-7034 Trondheim, Norway*

Received 25 October 1995; accepted in revised form 22 March 1996

Abstract. A particular case of interface cracks is considered. The materials at each side of the interface are assumed to have different yield strength and plastic strain hardening exponent, while elastic properties are identical. The problem is considered to be a relevant idealization of a crack at the fusion line in a weldment. A systematic investigation of the mismatch effect in this bi-material plane strain mode I dominating interface crack has been performed by finite strain finite element analyses. Results for loading causing small scale yielding at the crack tip are described. It is concluded that the near-tip stress field in the forward sector can be separated, at least approximately, into two parts. The first part is characterized by the homogeneous small scale yielding field controlled by J for one of the interface materials, the reference material. The second part which influences the absolute value of stresses at the crack tip and measures the deviation of the fields from the first part can be characterized by a mismatch constraint parameter M. Results have indicated that the second part is a very weak function of distance from the crack tip in the forward sector, and the angular distribution of the second part is only a function of the plastic hardening property of the reference material.

1. Introduction

Many of the studies on the fracture of weldments in the literature have neglected the presence of heat affected zones (HAZ) and placed the crack in the center of weld metal which is surrounded by base metal [1, 2]. However, experimental studies have indicated that an interface crack between the weld metal and heat affected zone (HAZ) may be the most critical one [3, 4]. In many cases, the crack in a weldment can be idealized as a bi-material (weld metal and HAZ or weld metal and base metal), interface crack or a tri-material (weld metal, HAZ and base metal) crack, see Figure 1.

Current standards for failure assessment based on fracture mechanics were developed for homogeneous materials and can not be directly applied to the assessment of fracture behavior of

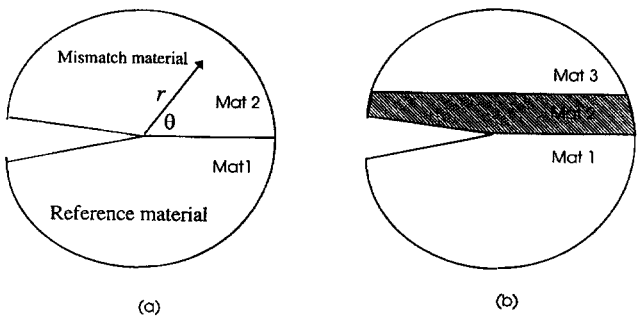

Figure 1. Idealization of cracks in weldments, (a) bi-material crack, (b) tri-material crack.

weldments. In a weldment, there are two constraints which invalidate the fracture mechanics parameters. They are the constraint caused by geometry and the constraint caused by the heterogeneous material properties or material mismatch. In order to predict the weldment toughness and to understand the fracture behavior of high strength steel weldments and particularly the effect of mismatch conditions, it is essential to investigate the interface crack-tip fields and the constraint caused by material mismatch. In this study, only the bi-material interface crack (Figure 1a) is studied. Study of the tri-material crack is currently being carried out.

The linear elastic solution for a general bi-material interface crack predicts rapid oscillation of the near-tip fields when the crack tip is approached. Here a 'general' interface crack implies that the bi- material constant ε is not zero (the elastic properties for both materials are different), where ε is defined as [5, 6]

$$\varepsilon = \frac{1}{2\pi} \ln \left[\frac{\frac{3-4\nu_1}{\mu_1} + \frac{1}{\mu_2}}{\frac{1}{\mu_1} + \frac{3-4\nu_2}{\mu_2}} \right] \tag{1}$$

and μ_i, ν_i are the shear moduli and Poisson's ratio for material i. With respect to the coordinate system shown in Figure 1(a), the linear elastic near-tip field for an interface crack can be written as

$$\sigma_{ij}(\theta, r) = \frac{1}{\sqrt{2\pi r}} [\mathrm{Re}\{\boldsymbol{K} r^{i\varepsilon}\} \tilde{\sigma}_{ij}^{I}(\theta, \varepsilon) + \mathrm{Im}\{\boldsymbol{K} r^{i\varepsilon}\} \tilde{\sigma}_{ij}^{II}(\theta, \varepsilon)], \tag{2}$$

where $\boldsymbol{K}$ is the complex stress intensity factor, and $\tilde{\sigma}_{ij}^{I}(\theta, \varepsilon)$ and $\tilde{\sigma}_{ij}^{II}(\theta, \varepsilon)$ are the universal dimensionless angular functions which depend on the elastic bi-material constant ε. For the problem considered, we assume that the elastic properties above and below the interface are the same, i.e. $\varepsilon = 0$. When $\varepsilon = 0, \tilde{\sigma}_{ij}^{I}(\theta, \varepsilon)$ and $\tilde{\sigma}_{ij}^{II}(\theta, \varepsilon)$ reduce to the standard mode I and II functions for homogeneous material. In other words, the elastic near-tip field for a bi-material crack with $\varepsilon = 0$ is equivalent to the homogeneous case. In a steel weldment, the elastic properties for base metal, weld metal as well as HAZ materials are usually assumed to be the same.

In the literature it has been claimed that the crack-tip fields for a general interface elastic-plastic crack are not of the usual separate form [5, 6]. Nevertheless, there are strong similarities between them and the mixed mode I and II fields for cracks in homogeneous materials. For the elastic-plastic interface crack case with elastic constant $\varepsilon = 0$, Shih and Asaro [5, 6] proposed that the near-tip field can be organized in the form

$$\sigma_{ij} = \sigma_0 \left(\frac{J}{\alpha \sigma_0 \varepsilon_0 r} \right)^{1/n+1} h_{ij} \left(\theta, \frac{r}{J/\sigma_0}, n \right), \tag{3}$$

where the material constants are for the weak material, J is the J-integral and h_{ij} is a bound function which changes slowly with respect to $r/(J/\sigma_0)$.

Recently results by Aoki et al. [7] have concluded that for an elastic- plastic interface crack with $\varepsilon = 0$, the stress distributions at various load levels with and without microvoid damage can be superimposed by normalizing the distance from the crack tip by the J-integral and that the J-integral is path-independent except for the immediate vicinity of the crack tip.

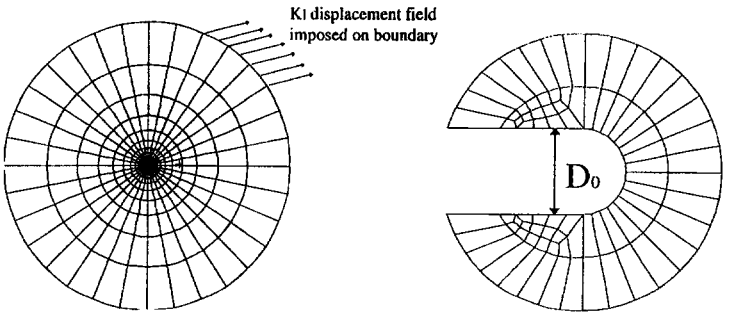

Figure 2. Small scale yielding modified boundary layer model, (a) global mesh, (b) crack-tip mesh arrangement.

Wide plate analysis results by Minami et al. [3] have indicated that crack-opening stress distributions along the fusion line for different mismatch conditions under the same loading level are similar to each other.

All these investigations indicate that for the elastic-plastic interface crack ($\varepsilon = 0$), the J-integral still sets the size scale of the zone of high stresses and strains and is still a useful fracture mechanics parameter. However, the exact stress level in front of the crack is influenced by the mismatch conditions. We define the deviation of the mismatched stress fields from the homogeneous stress field for one material (the reference material) as the constraint caused by mismatch. A quantitative assessment of the mismatch effect on the constraint is the purpose of this study. Detailed investigations show that stress fields in the forward sector can be, at least approximately, separated into two parts. The first part is the homogeneous small scale yielding field for the reference material, which can be characterized by the *HRR* theory. Here *HRR* is the widely accepted term in nonlinear fracture mechanics. The second part can be separated into a function of mismatch constraint parameter M and an angular function which depends only on the property of the reference material. It is demonstrated that M is a measure of the constraint caused by the material mismatch and is practically independent of the normalized distance to the crack tip.

2. Numerical procedure

The problem considered in this study is a plane strain crack at the interface between two infinite dissimilar materials with the same elastic properties. Small scale yielding is invoked. Here small scale yielding is defined such that the plasticity zone is embedded within the region where the asymptotic elastic field dominates the crack-tip field. A modified boundary layer (MBL) model (Figure 2) is applied for studying. The remote boundary displacements are given by the elastic asymptotic stress field of plane strain mode I crack

$$\begin{aligned} u(r,\theta) &= K_{\mathrm{I}}\frac{1+\nu}{E}\sqrt{\frac{r}{2\pi}}\cos(\tfrac{1}{2}\theta)(3-4\nu-\cos\theta), \\ \nu(r,\theta) &= K_{\mathrm{I}}\frac{1+\nu}{E}\sqrt{\frac{r}{2\pi}}\sin(\tfrac{1}{2}\theta)(3-4\nu-\cos\theta), \end{aligned} \tag{4}$$

where $K_{\mathrm{I}} = \sqrt{EJ/1-\nu^2}$ under plane strain condition, r and θ are polar coordinates centered at the crack tip with $\theta = 0$ corresponding to the interface.

The materials below and above the interface are indicated as reference material (material 1) and mismatch material (material 2), respectively (Figure 1). The yield stress for the reference material (σ_{10}) is fixed in the calculations. The elastic properties for the two materials are taken as $E/\sigma_{10} = 500$ and $\nu = 0.3$. In the present work, rate-independent power law strain hardening materials were assumed. For a material

$$\sigma_i = \sigma_{i0}\left(1 + \frac{\bar{\varepsilon}_i^p}{\varepsilon_{i0}}\right)^{n_i}, \tag{5}$$

where σ_i is the flow stress, $\bar{\varepsilon}_i^p$ is the equivalent plastic strain, σ_{i0} is the yield stress, ε_{i0} is the yield strain $\varepsilon_{i0} = \sigma_{i0}/E$, and n_i is the strain hardening exponent for material i.

The finite element meshes in the global scale and at crack tip are shown in Figure 2. There are a total of 1906 8-node elements and 5893 nodes. Finite deformation formulations with reduced integration scheme in ABAQUS were used. The crack tip is assigned a finite root radius. The initial notch radius is 5×10^{-5} times the radius of the MBL model. Another initial notch radius, 0.5×10^{-5} times the model radius has been tested and we found that once the crack tip has been blunted to about 2 times the initial notch radius, the solutions do not depend on the initial notch radius, i.e. the fields are almost self-similar (see Figure 3). Figure 3 shows the self-similar results for the case with $\sigma_{20}/\sigma_{10} = 1.5, n_1 = 0.1$ and $n_2 = 0.2$. Similar findings have been reported by O'Dowd and Shih [8, 9] for homogeneous material and by Asaro et al. [10] for inhomogeneous material. Due to reduced computing time, the notch tip radius, 5×10^{-5} times the radius of the model has been used.

The computed J-integral by ABAQUS has been compared with the applied J-integral (loading) to the MBL model. A strong path dependence has been shown in the finite-strain zone, but the J-integral becomes practically path-independent beyond the zone of finite strains. Similar findings have been reported in [7] for interface cracks with and without microvoid damage. There are differences between the computed J-integral of the homogeneous case and those of the mismatch cases in the finite strain zone. However, the differences are reasonably small for the weak plastic hardening materials for the contours with mean radius $r/(J_{\text{applied}}/\sigma_0) > 1$. For cases with $n_1 = 0.1$ and $n_2 = 0.1$ studied in the paper the error ranges from -6 percent to 3 percent. The overmatch cases overestimate the J-integral compared with the homogeneous case, while the undermatch cases are just the opposite. When the plastic hardening exponents increase, the computed J agrees better with the applied one. In order to facilitate the calculations of the different stress fields, the applied J has been used in the presentation of the results.

For simplicity, in the following, m is defined as the ratio of the yield stresses between the mismatch material and the reference material

$$m = \frac{\sigma_{20}}{\sigma_{10}}. \tag{6}$$

Thus a combination of m, n_1, n_2 uniquely define an interface crack. It must also be noted that the subscript 1 in the following stands for the 'maximum principal stress'. The subscript 'applied' has been omitted for the J-integral , and therefore J in the following means the applied J.

3. Results for small scale yielding

The results reported here are from the integration points. Polar coordinates, r, θ have been used and all the stresses are normalized by the yield stress of the lower part material, σ_{10}.

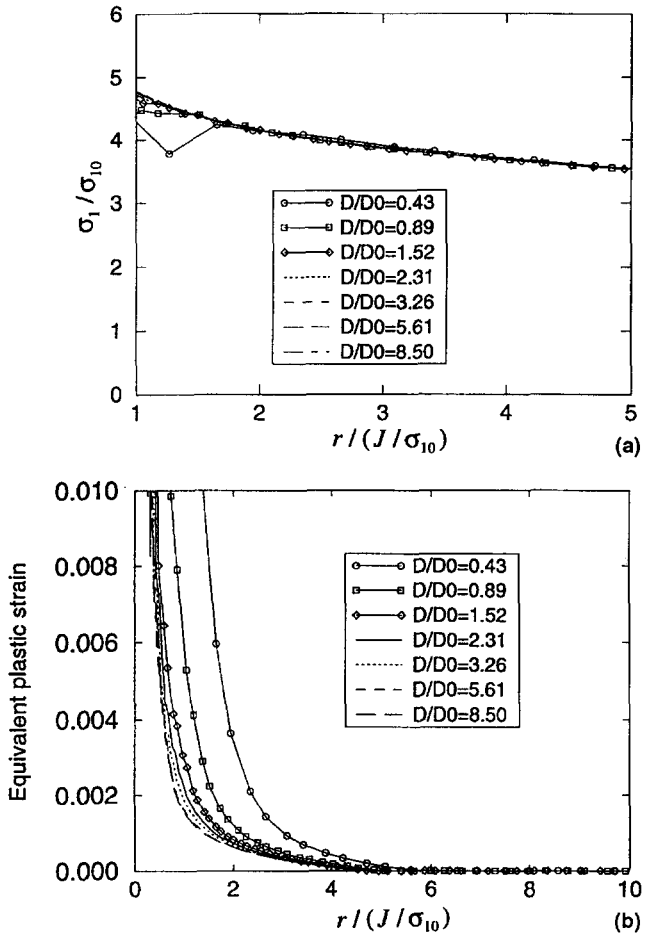

Figure 3. Solutions at different loading stages for the case $\sigma_{20}/\sigma_{10} = 1.5, n_1 = 0.1, n_2 = 0.2$. (a) is for the normalized maximum principal stress in the mismatch material at $\theta = 2.37°$, and (b) for the equivalent plastic strain in the reference material at $\theta = -2.37°$. In the figures, D0 is the initial notch opening, D is the notch opening displacement.

Two kinds of mismatches have been considered separately, i.e. yield stress mismatch with the same plastic strain hardening and plastic strain hardening mismatch with the same yield stresses. For the first kind of mismatch, two constant plastic hardening exponents have been examined, both $n_1 = n_2 = 0.1$ and 0.2. In each case, six mismatch sub-cases have been calculated with $m = 2, 1.75, 1.5, 1.25, 0.85$ and 0.75. For the plastic hardening mismatch, the case with $m = 1$ and $n_1 = 0.1, n_2 = 0.2$ has been studied. A general case with both yield stress mismatch and plastic hardening mismatch has also been examined. The cases considered are documented in Table 1. The ranges cover many of the practical situations in a steel weldment.

The results are presented first as a function of the similarity length scale $(r/(J/\sigma_0))$, in the range $1 \leqslant r/(J/\sigma_0) \leqslant 5$. In the range $r/(J/\sigma_0) < 1$, finite strain effect dominates, the solution is not compared. The range $1 \leqslant r/(J/\sigma_0) \leqslant 5$ has been selected since this zone encompasses the microstructually significant length scales for both brittle and ductile fracture. The objective is to sample the stress field at locations outside the finitely deformed

Table 1. Mismatch cases considered in the study

Yield stress mismatch	$m = 2.0$
	$m = 1.75$
	$m = 1.5$
	$m = 1.0$
$n_1 = n_2 = 0.1$ and $n_1 = n_2 = 0.2$	$m = 1.25$
	$m = 0.85$
	$m = 0.75$
Hardening mismatch, $m = 1$	$n_1 = 0.1, n_2 = 0.2$
General mismatch	$m = 1.5, n_1 = 0.1, n_2 = 0.2$

zone $r \geqslant 2\delta \approx r/(J/\sigma_0)$, but within the process zone applicable for cleavage fracture ($r \leqslant 8\delta$) [11], where δ is the crack-tip opening displacement. Angular distributions of the stress fields at selected distances to the crack tip have also been examined.

In addition to the radial and angular variations of the stress fields presented, the difference fields between the mismatch cases and the homogeneous solution of the lower part material, the reference material, have been calculated and displayed in the corresponding figures

$$\frac{\Delta\sigma_{ij}^{M}}{\sigma_{10}} = \frac{\sigma_{ij}^{M} - \sigma_{ij}^{\text{Ref.}}}{\sigma_{10}}, \tag{7}$$

where σ_{ij}^{M} represents the crack-tip field for a mismatch case and $\sigma_{ij}^{\text{Ref.}}$ denotes the reference field taken from the homogeneous small scale yielding solution for the lower part material. The M in σ_{ij}^{M} and $\Delta\sigma_{ij}^{M}$ is omitted in the figures for simplicity of presentation.

3.1. YIELD STRESS MISMATCH

3.1.1. $n_1 = n_2 = 0.2$

The radial variation of the stress components, $\sigma_{\theta\theta}, \sigma_{rr}$ and $\sigma_{r\theta}$ along with the maximum principal stress, σ_1 is presented for the six mismatch cases together with the homogeneous solution in Figure 4 at four different angles. The corresponding difference fields for the six mismatch cases are also shown in the same figures. $\theta = \pm 2.37°$ represents the (integration points) lines closest to the interface in the upper part and lower part materials, respectively. It can generally be seen that overmatch of the upper part material to the lower part material raised the normal stress levels in both sides of the interface. The undermatch effect is just the opposite. The singularity of the stress fields is more or less the same as the homogeneous one. However, the distributions of the stresses in the upper and lower parts are not symmetric. The differences of $\sigma_{\theta\theta}$ at $\theta = -45°$ are much smaller than those at $\theta = 45°$. We have also found that at $\theta = 45°$, mismatch has a very minor effect on σ_{rr}. Considering the angular distributions of the stresses below, it will be noticed that $\theta = 45°$ is close to a special position where mismatch has almost no effect on the difference field of σ_{rr}.

By examining the difference field of $\sigma_{\theta\theta}$, it is interesting to find that it has a very weak dependence on the normalized distance, especially when the mismatch ratio is not very severe

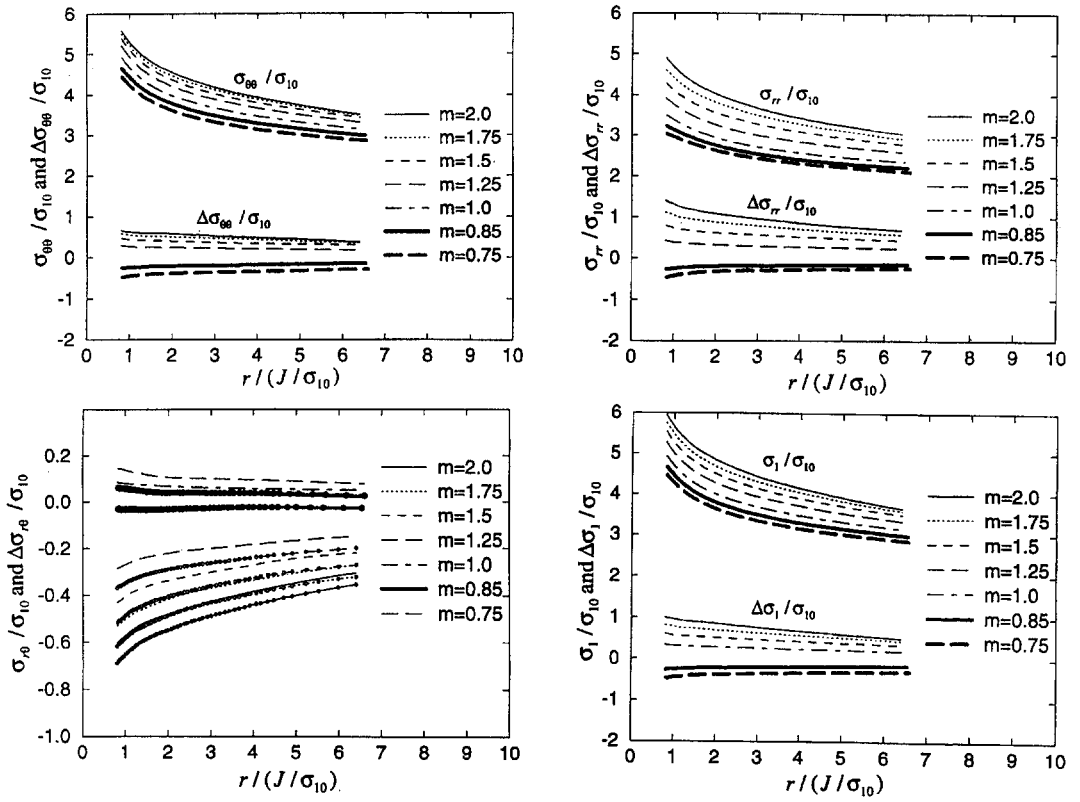

Figure 4a.

(less than 1.5). Similar behavior is seen in the fields for other stress components at the four angles examined.

Figure 5 displays the angular variations of the stress fields and their difference fields for all the cases at distance $r/(J/\sigma_0) = 2$. This distance has been suggested for the definition of Q [11]. The distributions at $r/(J/\sigma_0) = 4$ have also been examined and, as can be expected from the radial distribution results, no significant difference was found. First we observe that the difference fields have a strong dependence on the angle. It is found that $\sigma_{\theta\theta}$ is continuous across the interface and that there is a jump in σ_{rr}. The mismatch has elevated $\sigma_{\theta\theta}$ more on the strong material side than in the weak material side. This tendency is opposite for σ_{rr}. It is interesting to note that changing the mismatch parameter of the upper part material has greatly influenced the σ_{rr} in the lower part, however, the influence on the upper part itself is not significant. From Figure 5 we can observe that stress σ_{rr} around about $\theta = 25°$ is almost constant in all the six cases examined. This is the special position which has been mentioned in the radial distribution discussed above. We can also notice that the maximum value of the maximum principal stress appeared in the weak material, nevertheless the absolute maximum difference values in both sides of the interface are nearly the same.

The absolute amplitudes of the difference fields depend on the mismatch properties. However, the functional dependence of the difference fields for all the mismatch cases are very similar to each other. It has been realized that it could be possible to normalize these angular functions by dividing difference fields by the corresponding maximum values of the difference

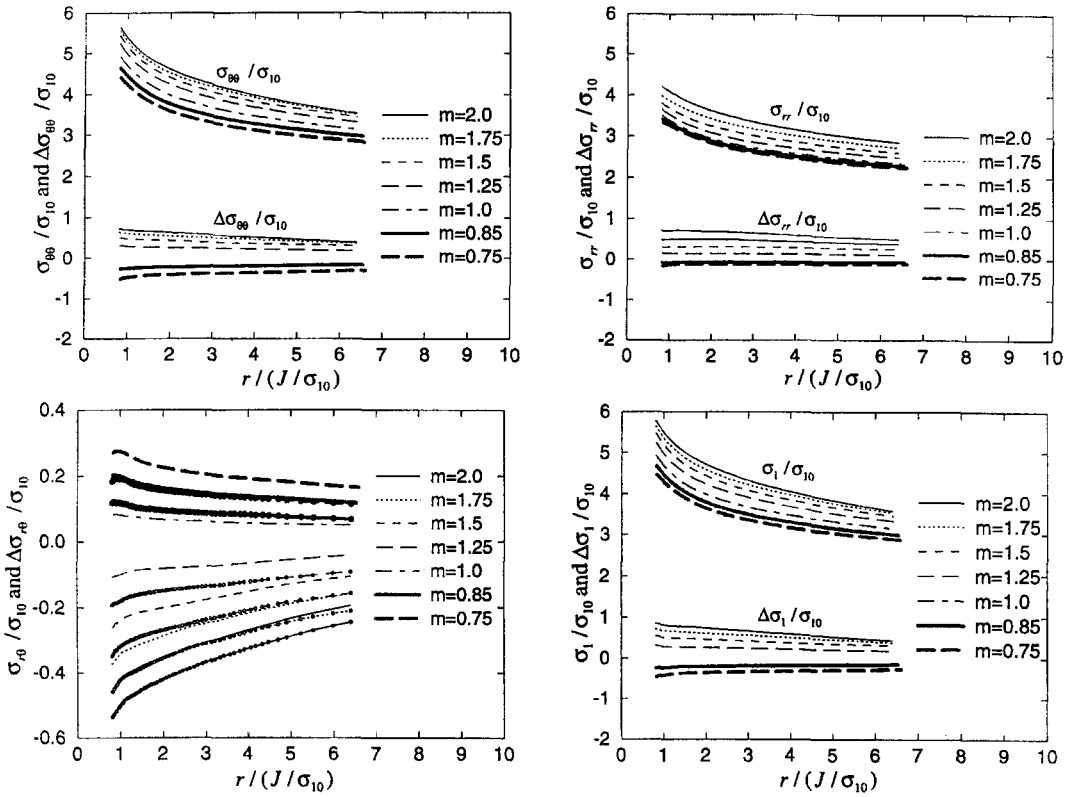

Figure 4b.

fields. This gives the normalized functions f_{ij} as shown in Figure 6. The amplitudes were taken from the reference material (lower part) for all the stresses except the $\sigma_{\theta\theta}$ which has only one maximum value in the mismatch material (see the discussion of the shape of the normalized functions below). Quite good consistent functions for the stress components and the maximum principal stress have been obtained.

We note from Figure 6 that $f_{\theta\theta}$ has only one maximum point which appears in the mismatch material. There are two local maximum points in f_{rr} and the global maximum point appears in the reference material. The function for the maximum principal stress f_1 is similar to f_{rr}, but the two maximum points have nearly the same value. The normalized function $f_{r\theta}$ has the maximum in the reference material. The normalized functions correspond better with each other in the reference material but slightly worse in the mismatch material. We recall that in the calculation of the difference fields, we used the lower part material as the reference material, because the purpose was to see how the stress fields in the lower part material are affected by the property of the upper part material. We also note that the reference field in (7) is derived from the homogeneous solution for the reference material.

Figure 6 shows that, in general, undermatch and overmatch have nearly the same function shapes but an angular shift can be noticed. It is found that the following transformation (for the undermatch cases)

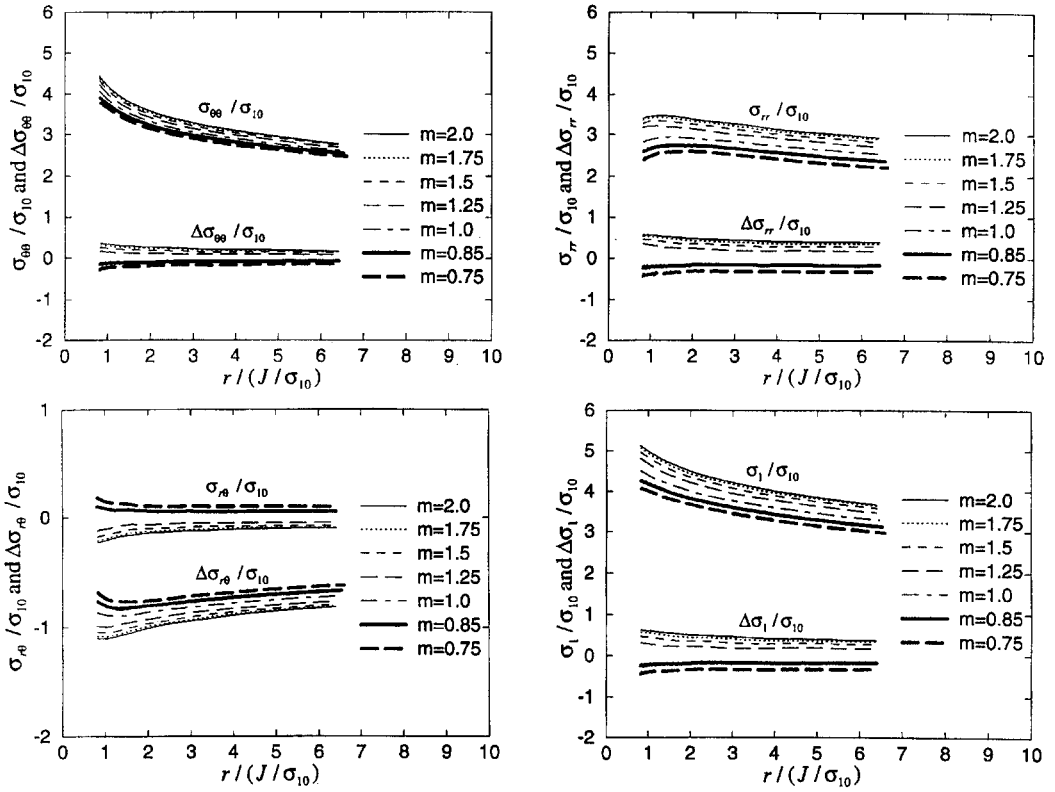

Figure 4c.

$$\begin{aligned} \tilde{f}_{ij}^{\text{over}}(\theta) &= f_{ij}^{\text{over}}(\theta) && \text{overmatch,} \\ \tilde{f}_{ij}^{\text{under}}(\theta) &= f_{ij}^{\text{under}}(\theta - 12) && \text{undermatch,} \end{aligned} \tag{8}$$

gives better consistent functions. Figure 7 shows the corrected normalized functions $\tilde{f}_{ij}^{\text{over}}$ and $\tilde{f}_{ij}^{\text{under}}$. This behaviour suggests that the angular dependence for the stresses can be normalized so that one unique function $\tilde{f}_{ij}$ can be used for both overmatch and undermatch cases such that

$$\begin{aligned} f_{ij}^{\text{over}}(\theta) &= \tilde{f}_{ij}(\theta), \\ f_{ij}^{\text{under}}(\theta) &= \tilde{f}_{ij}(\theta + 12). \end{aligned} \tag{9}$$

The maximum values of the difference fields M_{ij} used for the normalization are shown in Figure 8 as a function of m. It must be noted that $M_{r\theta}$ in Figure 8 is -2 times the maximum difference value of $\sigma_{r\theta}$ in Figure 6. As mentioned before, except $\sigma_{\theta\theta}$, all the other maximum difference values were taken from the lower part material. It can be observed that the maximum difference value for σ_{rr} deviates from the others when the m is larger than 1.5. However, when m is smaller than 1.5, the amplitudes of the stress difference fields M_{ij} and M_1 can be identified by a common parameter M which is a function of the mismatch ratio m.

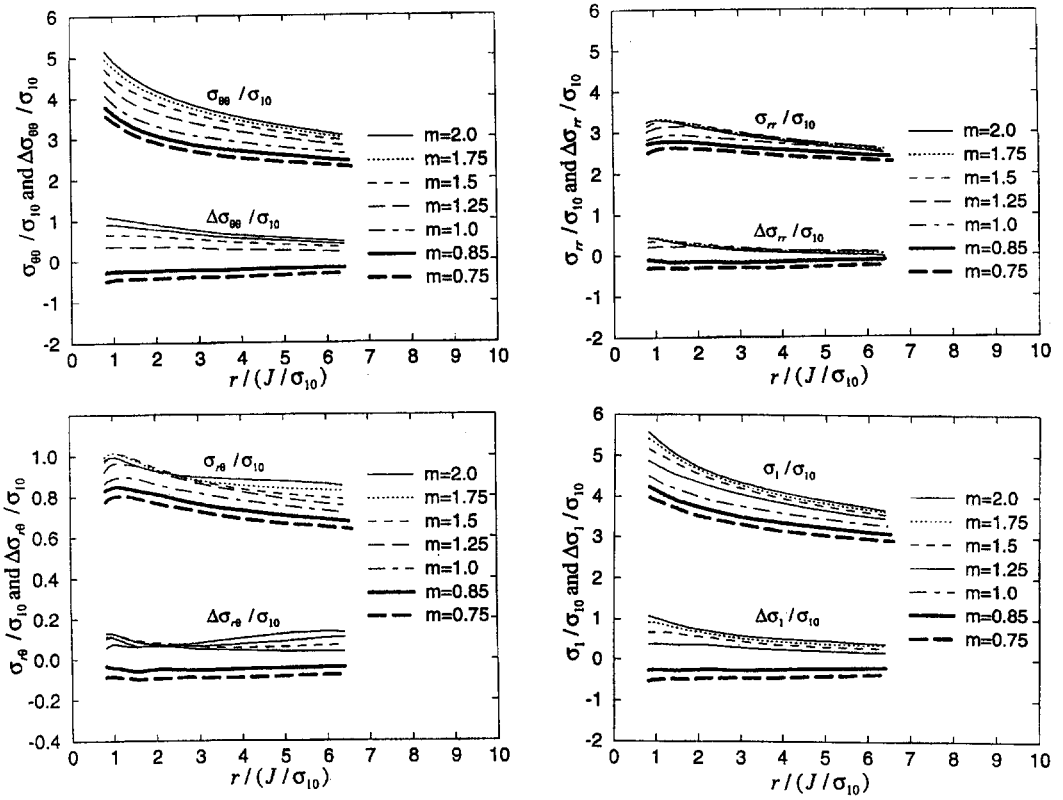

Figure 4d.

Figure 4. Radial distribution of the normalized stress fields and their difference fields at four angles, (a) $\theta = -2.37°$, (b) $\theta = 2.37°$, (c) $\theta = -45°$ and (d) $\theta = 45°$ for the cases with $n_1 = n_2 = 0.2$. σ_1 is the maximum principal stress. The lines with circles in Figure 4a and 4b represent the difference fields.

3.1.2. $n_1 = n_2 = 0.1$

The angular distributions of the stresses and their corresponding difference fields for the cases with plastic hardening components $n_1 = n_2 = 0.1$ are shown in Figure 9. In order to save space, the radial distributions were not presented. Very similar results to the cases with $n_1 = n_2 = 0.2$ have been found. The corrected normalized functions $\widetilde{f}_{ij}$ using the 12 degree shift (8) are shown in Figure 10. By comparing with Figure 8 and Figure 10, indeed the shapes of the normalized functions are very similar. However, it should be pointed out that the functions are not 'exactly' the same, because different reference fields have been used in subtracting the difference fields. Figure 11 shows the amplitudes of the difference fields M_{ij} and M_1, as a function of m. In general, the same conclusions to the cases $n_1 = n_2 = 0.2$ can be drawn.

3.2. PLASTIC STRAIN HARDENING MISMATCH AND GENERAL MISMATCH

In this section the effect of strain hardening mismatch and general mismatch on the difference fields has been investigated. The case for plastic hardening mismatch considered is with

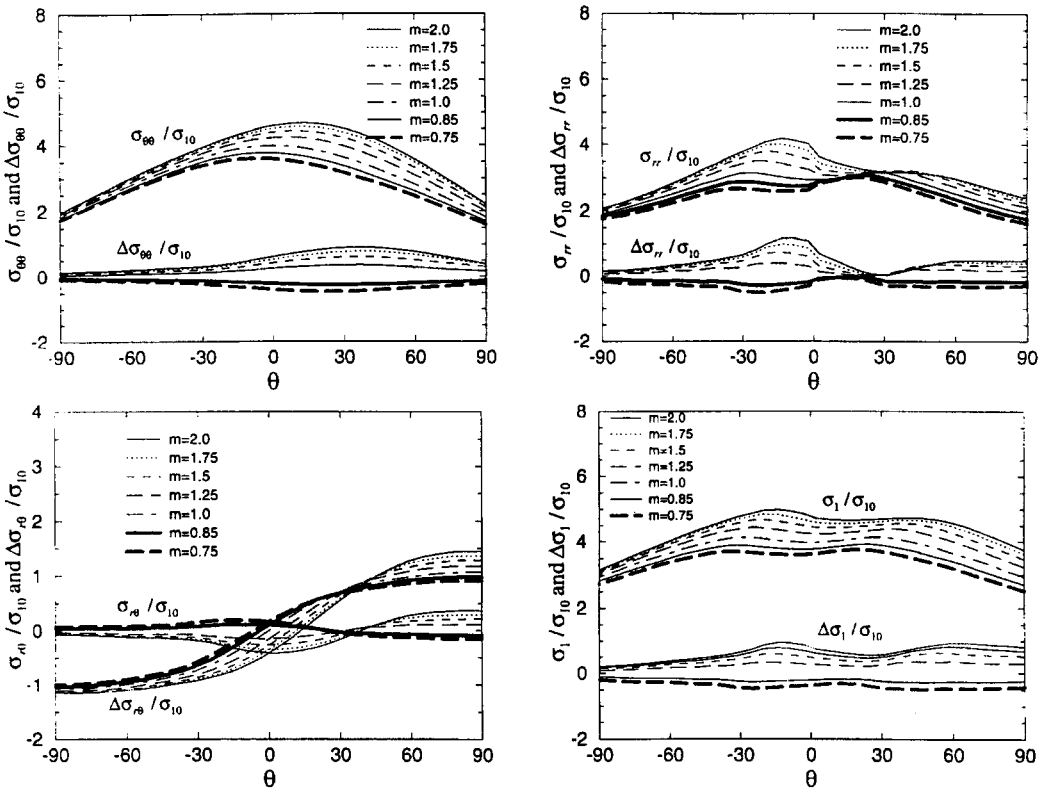

Figure 5. Angular variations of the normalized stress fields and their different fields at the distance $r/(J/\sigma_{10}) = 2$ for the cases with $n_1 = n_2 = 0.2$.

$m = 1.0, n_2 = 0.2, n_1 = 0.1$. The general mismatch case contains both yield stress mismatch, $m = 1.5$, and plastic hardening mismatch, $n_2 = 0.2, n_1 = 0.1$.

Similar weak dependence of the stress components on the normalized radial distance has been observed, see Figure 12 for the general mismatch case at $\theta = -2.37°$ and $\theta = -45°$, respectively. Figure 13 shows the normalized angular functions for the plastic hardening mismatch and general mismatch cases together with the functions for the case with $n_1 = n_2 = 0.1$ and $m = 1.5$. Surprisingly, as far as the lower part material is concerned, the three pairs of normalized functions are consistent with each other to a large extent. Figure 13 indicates that the normalized angular functions for overmatch cases can be approximately used for the plastic hardening mismatch and general mismatch cases without angular shift. The M_{ij} and M_1 for the plastic hardening mismatch ($m = 1.0$) and the general mismatch ($m = 1.5$) are shown in Figure 14. Similar observations to the yield stress mismatch can be drawn for the two cases. It other words, the mismatch effects in all the cases considered can be treated in a consistent way as explored in the next section.

4. Approximate structure of the interface crack-tip stress field

4.1. STRUCTURES OF THE INTERFACE CRACK-TIP STRESS FIELD

The results in the last section can be summarized as follows. The near-tip stress fields can be separated into two parts. The first part is the solution for the homogeneous small scale

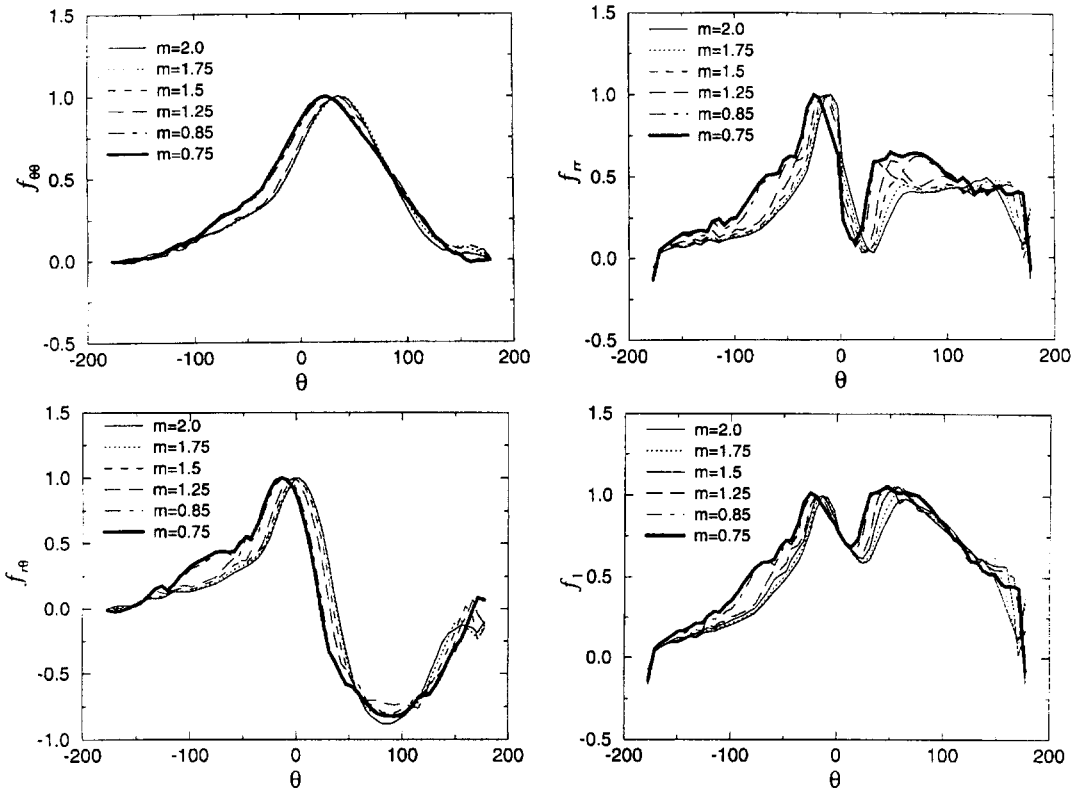

Figure 6. Normalized difference functions for the cases with $n_1 = n_2 = 0.2$.

yielding reference material which can be characterized by the *HRR* field and the second part measures the deviation of the stress fields under mismatch conditions from the reference case. The difference field in the forward sector is very weakly dependent on the radial distance (normalized) from the tip and can be approximately separated into one part which characterizes the mismatch propriety (M_{ij}) and another part which is a function of the angle and depends only on the plastic property of the reference material. The M_{ij} represents the amplitudes of the stress difference fields. Figures 8, 11 and 14 have shown that M_{ij} can be approximated by an unique constant M which characterizes the mismatch constraint. The angular dependence of the difference fields can be normalized for different mismatch conditions. Based on the above observations, the following formulations can be approximately constructed for the bi-material interface crack defined in the paper

$$\sigma_{ij}^{M}(r,\theta) = \sigma_{ij}^{\text{Ref.}}(n_1, J, r, \theta) + \sigma_{10} M(m, n_2) \bar{f}_{ij}(\theta + 12\beta, n_1) \tag{10}$$

where $\bar{f}_{rr}(\theta) = \tilde{f}_{rr}(\theta), \bar{f}_{\theta\theta}(\theta) = \tilde{f}_{\theta\theta}(\theta), \bar{f}_{r\theta}(\theta) = -0.5\tilde{f}_{r\theta}(\theta), \beta = 0$ for $m \geqslant 1$ and $\beta = 1$ for $m < 1$. In (10), $\sigma_{ij}^{\text{Ref.}}$ denotes the small scale yielding solution for the reference material, and the normalized angular functions depend only on the plastic property of the reference material. M is the amplitude of the angular difference fields which can be used for characterizing the material constraint caused by mismatch conditions. It can be seen from (10) that M is a function of the plastic hardening property of mismatch material n_2 and the mismatch ratio, m.

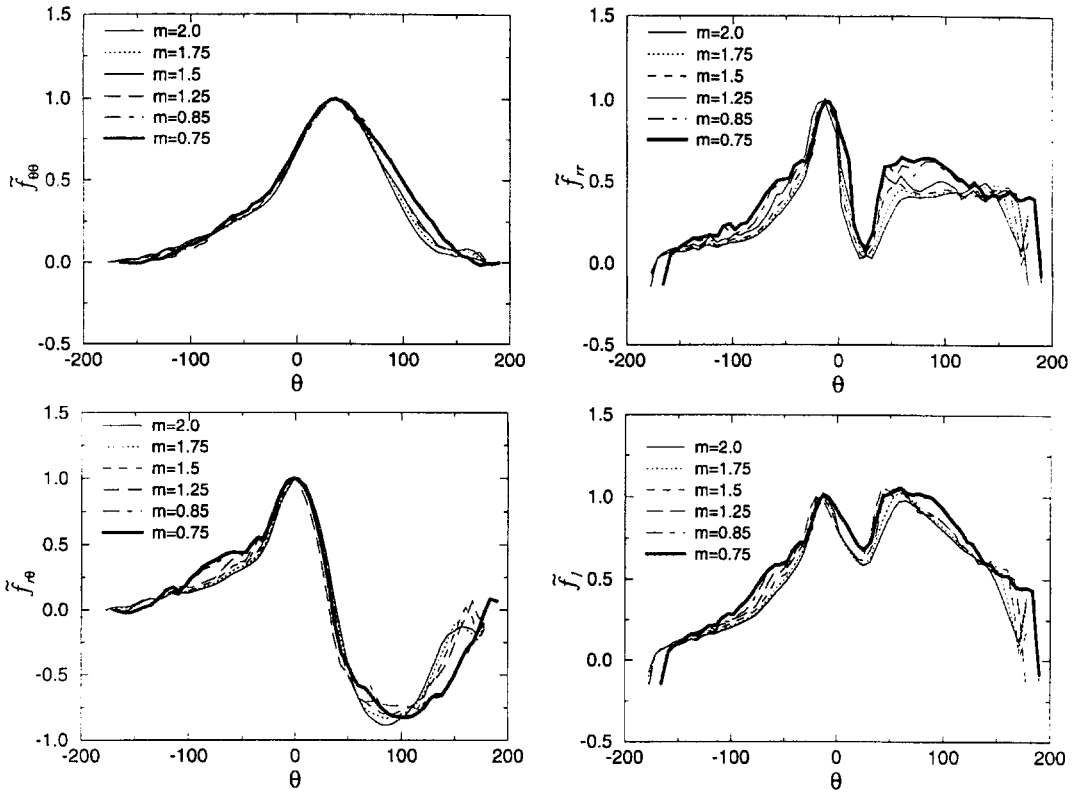

Figure 7. Corrected normalized functions for the cases with $n_1 = n_2 = 0.2$.

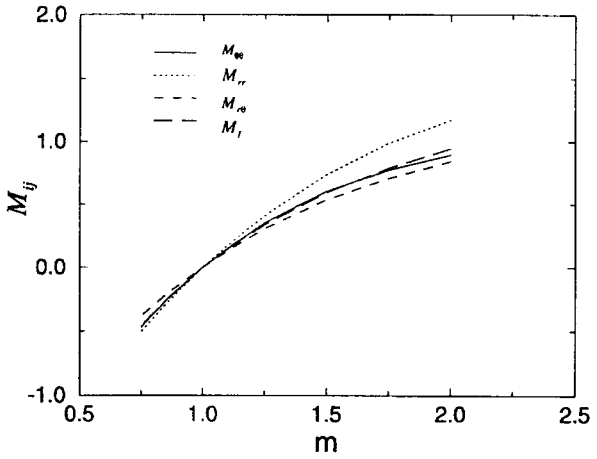

Figure 8. M_{ij} and M_1 as a function of the mismatch ratio m for the cases with $n_1 = n_2 = 0.2$.

Equation (10) applies for all mismatch cases considered and is most accurate in the range $-45° \leqslant \theta \leqslant 0°$ (in the reference material). Small scale yielding for the validity of the above formulations is assumed.

Equation (10) indicates that the stress fields for the interface crack can be characterized by two parameters J and M.

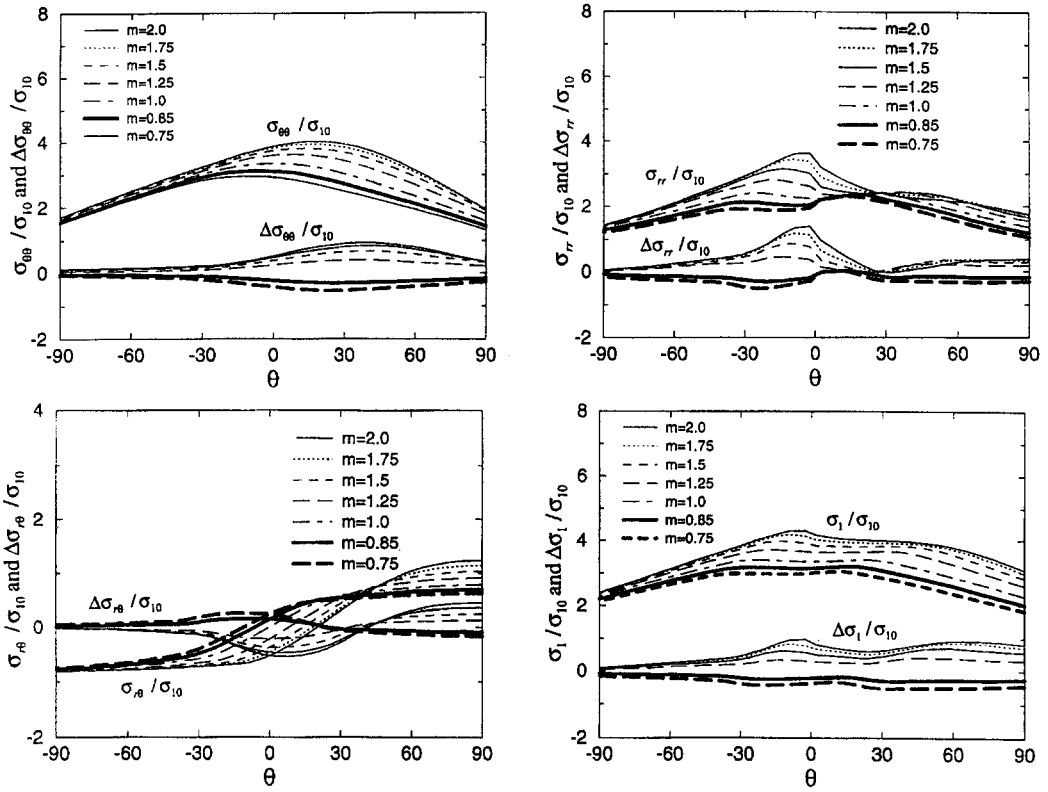

Figure 9. Angular variations of the normalized stress fields and thier different fields at the distance $r/(J/\sigma_{10}) = 2$ for the cases with $n_1 = n_2 = 0.1$.

4.2. How to determine the M

Figures 8, 11 and 14 show that M_{ij} are very close to each other except for M_{rr} when the m is larger than 1.5 or under plastic hardening mismatch conditions. The absolute value of M_{rr} is larger than the other components. However, the ratio between M_{rr} and the other components, for example, M_1, is rather constant, about 1.15, see Figure 15. Therefore, once M is determined from the other components, M_{rr} can be obtained, for example, by multiplying a constant, if more accurate formulation than (10) is required.

The M can be determined by evaluating the maximum principal stress at a fixed normalized distance, for example, $r/(J/\sigma_0) = 2$, for a mismatch case and comparing it with the homogeneous small scale yielding solution for the same part of material under investigation. The amplitude of the angular difference field is the M. The maximum principal stress is chosen for evaluating the M, because the distribution of $\tilde{f}_1$ has a maximum point in each side of the interface and the maximum values are very close to each other. It will not make large errors when the M is evaluated by the maximum difference value at the mismatch material side.

The evaluation of the homogeneous small scale yielding solution can be made by the *HRR* field or numerical solution. In our calculations, the numerical solution for the small scale yielding homogeneous field has been used. As the same nature of the Q fields [8, 9], the value of M is slightly affected by the choice of the reference field. If the reference field is changed from our numerical solutions to the *HRR* solutions, a small change must be applied to the M.

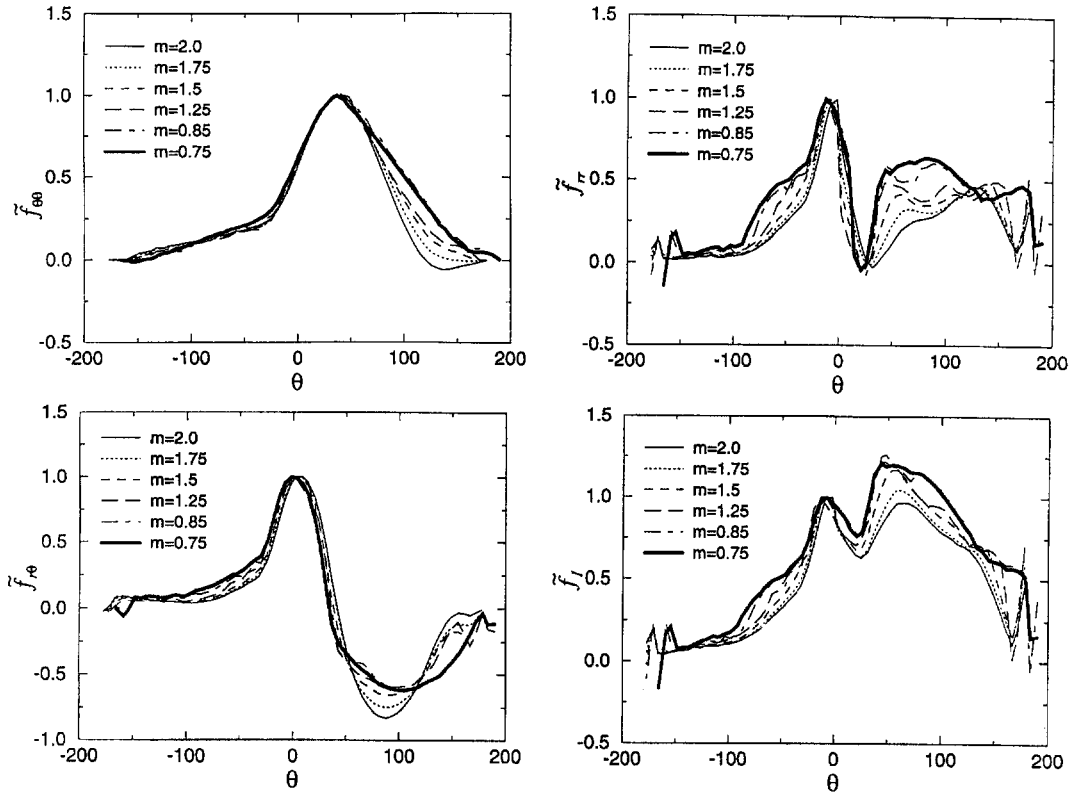

Figure 10. Corrected normalized functions for the cases with $n_1 = n_2 = 0.1$.

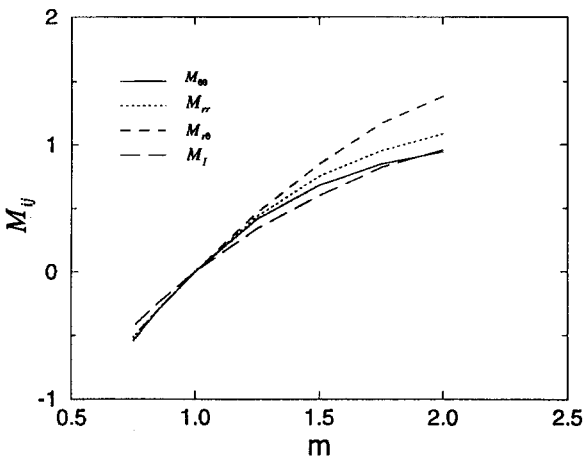

Figure 11. M_{ij} and M_1 as a function of the mismatch ratio m for the cases with $n_1 = n_2 = 0.1$.

5. Discussions

Results above have demonstrated that the small scale yielding stress fields in the bi-material interface crack tip can be separated into a field controlled still by the J and another field

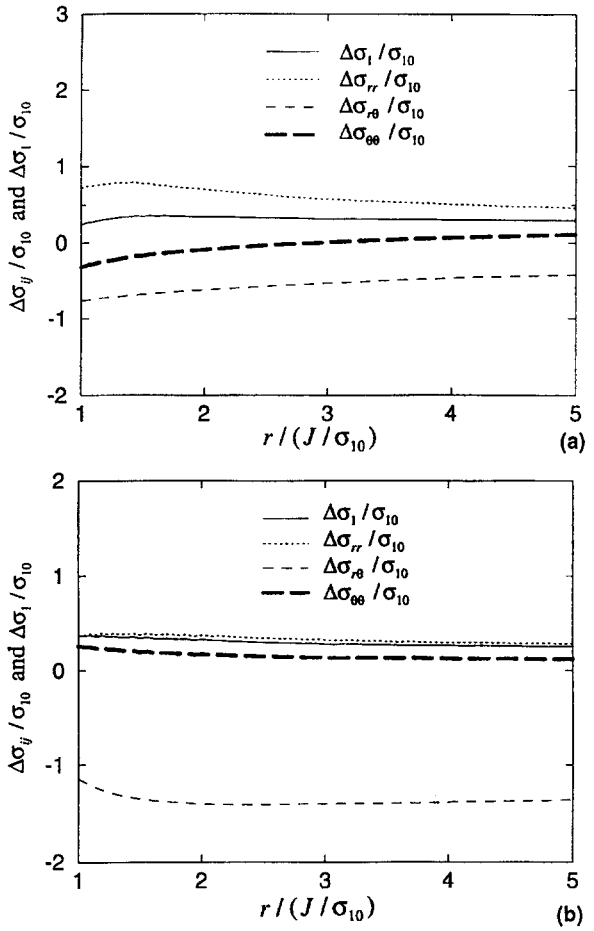

Figure 12. Radial distributions of the difference fields for the general mismatch case at (a) $\theta = -2.37°$ and (b) $\theta = -45°$.

characterized by the M. In the following some issues related to the M fields are summarized and discussed.

5.1. WHAT ARE THE M FIELDS?

M field is the field caused by material mismatch across the interface. It is a non-singular field. The field itself is complicated, but can be approximately separated into two parts, the first is practically independent of the normalized radial distance to the crack tip and the second part is an angular function which depends only on the property of the reference material. Once the reference material is chosen, the angular functions are known. In a practical application, the exact forms of the angular functions are not the most important, once the value of M is determined.

M is the dimensionless amplitude of the M fields. Together with J, the stress status in a bi-material interface crack can be determined.

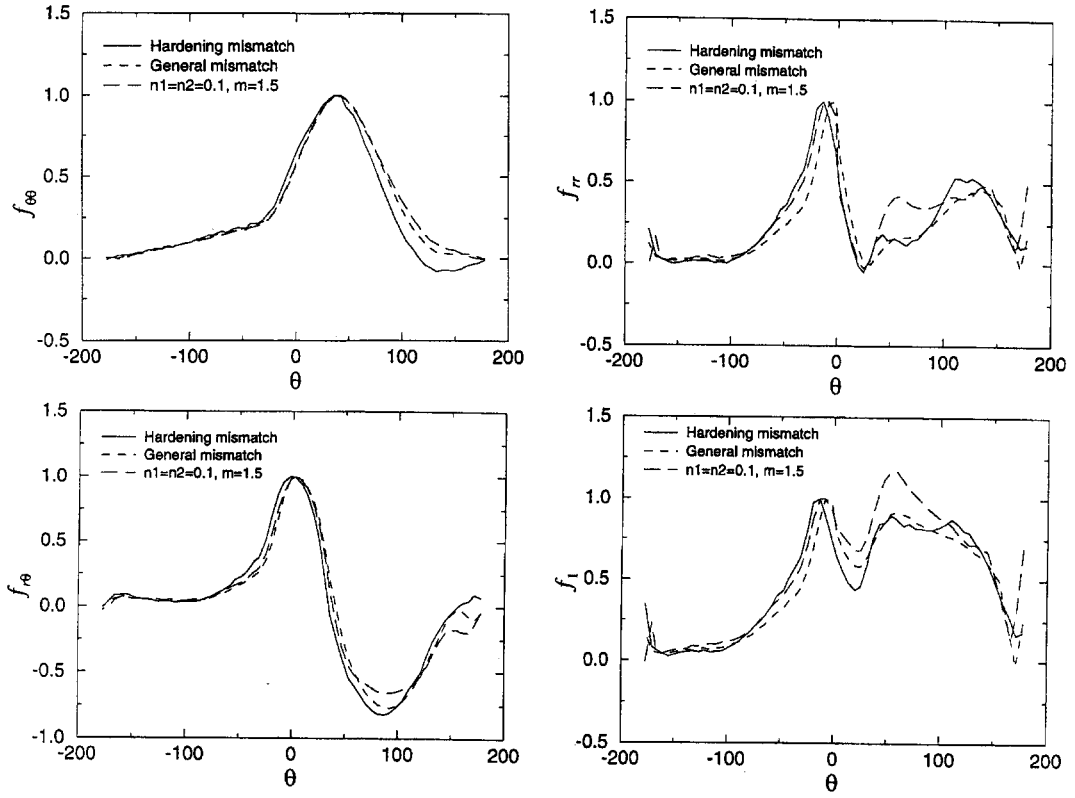

Figure 13. Normalized difference functions for the plastic strain hardening mismatch and the general mismatch cases.

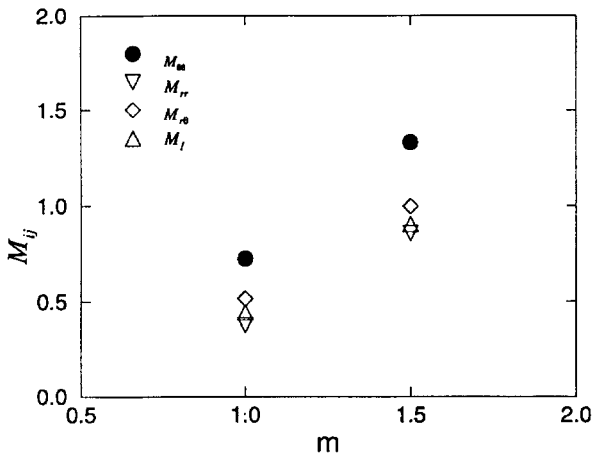

Figure 14. M_{ij} and M_1 for the plastic hardening mismatch ($m = 1.0$) and the general mismatch ($m = 1.5$).

5.2. THE SIGNIFICANCE OF THE M FIELDS

Cleavage fracture is usually controlled by critical levels of the hoop (opening) stress ahead of the crack tip acting over microstructurally significant distances. In a small scale yielding bi-material crack, the stress distribution and maximum stress are influenced by M alone while the

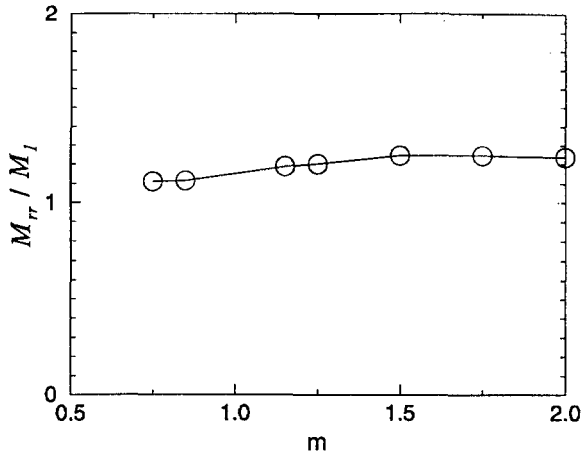

Figure 15. The ratio of M_{rr}/M_1 for the reference yield stress mismatch with $n_1 = n_2 = 0.2$ as a function of m.

scale of microstructurally significant distance is scaled by the J. By using a micromechanics criterion for the cleavage fracture, for example the RKR criterion [12], the J-M theory can predict variation of the cleavage toughness with mismatch properties [13]. In a weldment, if, for example, the HAZ is identified as the most critical material for cleavage fracture, the effect of changing the weld material properties on the HAZ stress field and toughness can be assessed. The application of the J-M theory to the assessment of the fracture behavior of weldments has been carried out and reported elsewhere [14, 15].

5.3. Comparison of the Q fields and the M fields

Q [8, 9] measures the constraint by geometry while M signifies the constraint by material property mismatch. $M$is introduced in this paper within the scope of small scale yielding and under the condition of zero Q.

There is a difference between the Q fields [8, 9] and the M fields. The Q fields were established by higher-order asymptotic analysis and are symmetric and do not change the shape of the stress contours but the size. Although M field is self-similar, it is not symmetric about the interface and will change both the shape and size of the stress contours.

An important problem which has not been discussed here is the combination of the constraints caused by geometry and the material mismatch. It is observed that the stress fields in the dual constraint case are still separable under certain conditions. A framework called J-Q-M theory has been formulated [16].

5.4. One limitation of the M fields

There is a limitation to the application of the J-M theory, (10). The limitation is about the stress-strain curves of the two materials. The general mismatch case reported in the paper had $m = 1.5, n_1 = 0.1, n_2 = 0.2$. It means that the low yield strength material has low plastic hardening capacity and the two stress-strain curves will never cross. Another general case with $m = 1.5, n_1 = 0.2, n_2 = 0.1$ has been analyzed. This case implies that the low yield strength material has higher plastic hardening capacity and the two curves cross at a plastic strain about 0.08 which is nearly 40 times the yield strain of the low yield strength material. The same

procedure as described in Section 3 has been used in subtracting the difference fields. Different distributions of the different fields, especially for σ_{rr}, were obtained and these different fields could not be normalized using the same functions as the other cases. Therefore, it is indicated that the J-M theory (10) is limited to the cases where the stress-strain curve does not cross each other.

References

1. R.H. Dodds, T.L. Anderson and M. Kirk, *International Journal of Fracture* 48 (1991) 1–22.
2. M.T. Kirk and R.H. Dodds, Effect of weld strength mismatch on elastic-plastic fracture parameters. Structural Research Series No. 570, University of Illinois at Urbana-Champaign, August, 1992.
3. F. Minami, M. Toyoda, C. Thaulow and M. Hauge, Effect of strength mis-match on fracture mechanical behavior of HAZ-notched weld joint. Proceedings of the 2nd Workshop on *Constraint Effects on the Structural Performance of Welded Joints*, September 1994, Osaka, Japan.
4. C. Thaulow, A.J. Paauw, M. Hauge, M. Toyoda and F. Minami, Fracture property of HAZ-notched weld joint with mechanical mis- matching – Part II. Mis-matching of welds, ESIS 17 1994, Mechanical Engineering Publications, London (1994) 417–432.
5. C.F. Shih and R.J. Asaro, *Journal of Applied Mechanics* 55 (1988) 299–316.
6. Ibid., 56 (1989) 763–779.
7. S. Aoki, K. Kishimoto and N. Takeuchi, *International Journal of Fracture* 55 (1992) 363–374.
8. N.P. O'Dowd and C.F. Shih, *Journal of the Mechanics and Physics of Solids* 39 (1991) 989–1015.
9. Ibid, 40 (1992) 939–963.
10. R.J. Asaro, N.P. O'Dowd and C.F. Shih, Elastic-plastic analysis of cracks on bimaterial interfaces: interfaces with structure. *Materials Science and Engineering* A162 (1993) 175–192.
11. R.H. Dodds, C.F. Shih and T.L. Anderson, Continuum and micromechanics treatment of constraint in fracture. *International Journal of Fracture* 64 (1993) 101–133.
12. R.O. Ritchie, J.F. Knott and J.R. Rice, *Journal of the Mechanics and Physics of Solids* 21 (1973) 395–410.
13. Z.L. Zhang, M. Hauge and C. Thaulow, Assessment of material mismatch constraint in a bi-material elastic-plastic interface crack. Presented at the 2nd International Symposium on Mis-matching of Welds, Geesthacht, Germany (1996).
14. Z.L. Zhang, C. Thaulow and M. Hauge, Effects of crack size and weld metal mismatch on the haz cleavage toughness of wide plates, *Engineering Fracutre Mechanics*, submitted.
15. Z.L. Zhang, C. Thaulow and M. Hauge, On the constraint effects in HAZ-cracked wide plate specimens. Presented at the 2nd international Symposium on Mis-matching of Welds, Geesthacht, Germany (1996).
16. Z.L. Zhang, M. Hauge and C. Thaulow, The effect of T stress on the near tip stress fields of an elastic-plastic interface crack. To be presented at the 9th International Conference on Fracture, Sydney, April 1–5, 1997.